Biosensors and Bioelectronics 79 (2016) 500–507

Contents lists available at ScienceDirect

Biosensors and Bioelectronics

journal homepage: www.elsevier.com/locate/bios

Aluminum nanopyramid array with tunable ultraviolet–visible–infrared wavelength plasmon resonances for rapid detection of carbohydrate antigen 199

Wanbo Li [a], Yongcai Qiu [b], Li Zhang [a], Lelun Jiang [a], Zhangkai Zhou [c], Huanjun Chen [c], Jianhua Zhou [a,*]

[a] Key Laboratory of Sensing Technology and Biomedical Instruments of Guangdong Province, School of Engineering, Sun Yat-sen University, Guangzhou 510006, China
[b] Department of Materials Science and Engineering, Stanford University, Stanford, CA 94305, United States
[c] State Key Laboratory of Optoelectronic Materials and Technologies, School of Physics and Engineering, Sun Yat-sen University, Guangzhou 510275, China

ARTICLE INFO

Article history:
Received 6 September 2015
Received in revised form
12 December 2015
Accepted 14 December 2015
Available online 17 December 2015

Keywords:
Localized surface plasmon resonance
Aluminum nanopyramid array
Ultraviolet–visible–infrared
Biosensing
Cancer biomarker

ABSTRACT

Aluminum-based localized surface plasmon resonance (LSPR) holds attractive properties include low cost, high natural abundance, and ease of processing by a wide variety of methods including complementary metal oxide semiconductor process, making itself having an edge over conventional ones induced by noble metal. However, the inherent drawbacks of plasmonic mode limited on UV–green wavelength, low refractive index sensitivity, as well as heavy-shape-dependence greatly prevent aluminum plasmonics from real-life biosensing. Here, we demonstrated a uniform quasi-3-dimensional Al nanopyramid array (NPA) structure with tunable ultraviolet–visible–infrared (UV–vis–NIR) plasmon resonances for biosensing. By changing the reflection measuring angle, we could easily obtain typical peaks simultaneously exhibited on the reflectance spectrum across UV–vis–NIR wave region. The Al NPAs carried out high refractive index sensitivities which even comparable with that of noble metal, and can be used as a biosensor for directly detecting cytochrome c and carbohydrate antigen 199 in air after the sensing surface was washed cleanly and dried; the limits of detection were determined to be 800 nM and 29 ng/mL, respectively. Our proposed work therefore initiates the low-cost, high-performance biosensing using aluminum plasmonics, which would find wide applications in rapid diagnosis, mobile-healthcare and environmental monitoring.

© 2015 Elsevier B.V. All rights reserved.

1. Introduction

Localized surface plasmon resonance (LSPR) in metallic nanostructures and nanoparticles has been playing a pivotal role in various fields, including sensing, imaging, color display, information processing, and energy harvesting, due to its unique and outstanding manipulation of light (Atwater and Polman, 2010; Schuller et al., 2010; Yokogawa et al., 2012). One of the most conspicuous applications empowered by such plasmonic resonance is biosensing, which is regarded as a crucial component for bio-interaction analysis, early diagnosis, and portable medical supervision in mobile healthcare (Free et al., 2013; Li et al., 2015). Recent years have seen achievements of exquisite size and shape control in the synthesis of noble metal nanoparticles (Ament et al., 2012; Guo and Kim, 2011; Sannomiya and Vörös, 2011) and nanostructures (Gordon et al., 2008; Li et al., 2015; Stewart et al., 2006; Wang et al., 2014) (i.e. gold, silver, and platinum), and their extensively applications in biological and chemical sensing. Unfortunately, the intrinsic properties and high price of these noble metals, as well as their incompatibility with the popular manufacturing scheme that incorporates complementary metal oxide semiconductor (CMOS) process, present significant limitations for their large-scale use (Lohse et al., 2014; O Brien et al., 2014; Schade et al., 2014). Moreover, for Au-mediated plasmonic resonance, interband transitions are supposed to cause a dissipative channel at wavelengths below 550 nm, while the nanostructures made of Ag are extremely vulnerable to color degradation resulting from oxidation and sulfidation (Naik et al., 2013; Tan et al., 2014). These factors practically prohibit the adoption of those precious metals as a material candidate for widespread use.

Meanwhile, aluminum (Al) holds attractive properties including low cost, high natural abundance, high stability (because of the surface oxidation layer), and ease of processing by a wide variety of methods including CMOS process, making Al LSPR having an

* Corresponding author.
E-mail address: zhoujh33@mail.sysu.edu.cn (J. Zhou).

http://dx.doi.org/10.1016/j.bios.2015.12.038
0956-5663/© 2015 Elsevier B.V. All rights reserved.

edge over conventional noble plasmonic materials (e.g. Au and Ag). Additional optimistic aspects of Al encompass neutral tint, broad resonance, and good adhesion to diverse substrates (Clausen et al., 2014; Knight et al., 2014; Olson et al., 2014; Zheng et al., 2014). Taking into account the aforementioned appeal of Al, researchers have paid increasing interests on exploring the possibility of biosensing on Al materials, such as surface enhanced fluorescence (SEF) (Chowdhury et al., 2009; Ray et al., 2007) and surface enhanced Raman scattering (SERS) (Liao and Stern, 1982; Zhang et al., 2006), by taking advantages of its excellent optical properties of LSPR in the region from deep ultraviolet (UV) electromagnetic spectrum (Knight et al., 2014). Despite its potential, the exploitations of Al in plasmonics, especially for refractometric biosensing, are still in their infancy and facing a variety of problems and challenges.

On one hand, recent investigations have been focused on tailoring the plasmonics into the deep UV region, which, when applied to biosensing, are beneficial for the SEF and SERS, however, bring about troubles for refractometric biosensing, including the photo-toxicity to biological components and the detection noise from absorption band and auto-fluorescence by bio-molecules, because UV or blue plasmons match the general electron transition energy for the organic molecules. On the other hand, Al plasmonic nanostructures have been rarely applied to refrectometric biosensing, owning to the limitations of low refractive index (RI) sensitivities of plasmon resonance located in the UV to green wave region (Barrios et al., 2014; Canalejas-Tejero et al., 2014; Norek et al., 2014; Skinner et al., 2008). The inhomogeneity of nanostructures, as well as the oxidization of outer Al layer (Bisio et al., 2014; Chan et al., 2008), decrease the RI sensitivity of Al nanostructure (Bisio et al., 2014; Langhammer et al., 2008). These impacts are even huge on the smaller NPs. The RI sensitivities of plasmonic Al nanostructures are not comparable with that of conventional noble metal, making it difficult for detection trace analytes with concentration range from pM to fM, which are crucial for rapid diagnosis. Therefore, Al plasmonic nanostructure with high RI sensitivities from UV to infrared wave regions for on-demand high-performance biosensing is still a challenge for real-life application.

Herein, we reported a uniform quasi-3-dimensional Al nano-pyramid array (NPA) structure with tunable ultraviolet–visible–infrared (UV–vis–NIR) plasmon resonances for biosensing. The Al NPA with large-area uniform nanosutructure was fabricated through an electrochemical etching method. By changing the reflection measuring angle, we could easily obtain typical peaks exhibited on the reflectance spectrum from UV–vis to NIR wave region. Taken as example, we conducted RI-resolved peak shifts of these LSPRs at 15°-measuring angle, and found that the Al NPAs hold high RI sensitivities which even comparable with that of Au plasmonics. We further demonstrated the Al NPA as a biosensor for one-step detecting cytochrome c (Cyt c) and carbohydrate antigen 199 (CA199) through nonspecific and specific interaction systems, with detection limits up to 800 nM and 29 ng/mL, respectively.

2. Materials and methods

2.1. Materials

Al foil with a thickness of 0.25 mm (99.99%) was bought from Alfa Aesa. Cytochrome c (Cyt c, from horse heart) was from Genview Scientific (US). 1-Ethyl-3-[3-dimethylaminopropyl] carbodiimide hydrochloride (EDC) was purchased from Fluka Analytical (US). N-Hydroxysuccinimide (NHS) and polyacrylic acid (PAA, molecular weight=350,000, 35 wt% in water) were supplied by Sigma Aldrich Company (US). NaH_2PO_4 and Na_2HPO_4 were from Da-Mao chemical reagent (Tianjin, China). Ethanol, glycerol, ethylene glycol, isopropyl alcohol, and acetone were obtained from Fuyu chemical reagent (Tianjin, China). Phosphoric acid, citric acid, chromic acid, and perchloric acid were all from Zhiyuan reagent (Tianjin, China). All chemicals and solvents were of analytical grade and were used as received. Phosphate buffer solutions (PBS, 0.1 M) were prepared by mixing the stock solutions of NaH_2PO_4 and Na_2HPO_4, and then adjusting the pH to 7.2 or 2.0. carbohydrate antigen 199 (CA199) antibody, CA199 antigen standards, and alpha-fetoprotein (AFP) antigen standards were all from Fapon Biotechnology (Shenzhen, China) and stored at 4 °C as received. Double distilled water was used throughout all experiments.

2.2. Fabrication of Al NPA substrate

The Al NPA substrate was prepared through denting and then electrochemical etching. A flat aluminum sheet was ultrasonically washed with acetone and isopropyl alcohol, and then was electrochemically polished in the mixture contained perchloric acid and ethanol (v:v=1:3) for 2 min at 10 °C. Then the Al sheet was dented using a silicon mold with square ordered pillar array on its surface with a pressure of approximately 2×10^4 N/cm^2. After that, the pattern was transferred to the Al sheet. The dented substrates were then anodized in 240 mL solution composed of citric acid (2 wt%) and ethylene glycol (2 wt%) and H_3PO_4 (0.01%) at 10 °C with a voltage of 400 V. The Al NPA substrate was finally obtained by etching away the anodization layer in a mixture of phosphoric acid (6 wt%) and chromic acid (1.8 wt%) at 63 °C for 40 min.

2.3. Measurements of the reflectance spectra

The measurements were taken on an ultraviolet/visible/near-infrared spectrometer (Lambda 950, PerkinElmer). The incidence angle of the spectrometer can be changed from 8° to 68° at an accuracy of 0.5°. All reflectance spectra were corrected by dividing them with the reflectance spectrum of a silver mirror, which served as a reference only.

2.4. Refractive index (RI) sensitivity measurements

RI sensitivity measurements were performed by submerging the Al NPA in aqueous solutions of glycerine (Gl) with different concentrations (0, 25.96, 41.46, 62.50, and 86.57 wt%), which is a standard procedure for calibration and determination of the bulk RI sensitivity. The RIs are 1.333, 1.355, 1.386, 1.417, and 1.447, respectively. To obtain the 15°-measuring angle in the solutions with different concentrations, we adjusted incident angle of the wave from spectrometer according to the Snell's Law $n_1 \sin\theta_1 = n_2 \sin\theta_2$. The NPA surface was rinsed thoroughly with deionized water after each measurement. Three spectral measurements at each concentration were performed for the standard deviation (s.d.) calculation.

2.5. Cyt c and CA 199 detection in air

The Al NPA was firstly cleaned with UV/O_3 for 15 min, and then was treated with PAA solution (0.02 M, pH 5.0) for 30 min. These treatments ensured that the entire Al_2O_3 surface was covered by a self-assembled PAA layer containing pendent carboxyl groups. The unreacted PAA molecules were washed away with sufficient phosphate buffer (pH=7.2) and deionized water sequentially. Unless it was noted, the same wash-off procedures were conducted before all reflectance measurements in the following Cyt c and CA199 detections.

For Cyt c detection, reflectance spectrum of the PAA-modified

NPA substrate was recorded as the reference. The surface of the NPA was treated with 20 μL Cyt c solution (10 μM, pH 7.2) for 5 min; then was washed thoroughly, and dried with nitrogen flow. After that, the reflectance spectrum was measured. The PAA-modified NPA was regenerated by washing it with PBS (pH 2.0) flow for 30 s. Adsorbed Cyt c molecules was released because the PAAs on the NPA surface were neutral or weak positive in acidic environment (pH 2.0). The peak position blue shifted to the one of reference spectrum, indicating that the PAA-modified NPA was ready for the next Cyt c detection. Cyt c solutions with different concentrations of 0.5, 0.8, 1, 5, 10, and 35 μM were employed for the concentration-dependent measurements. At each concentration, three spectral measurements were carried out for the s.d. calculation.

For CA199 detection, the PAA modified Al NPA was further functionalized with CA199 antibody through covalent binding. The –COOHs of the PAA on the surface of NPA were firstly activated using a 50 μL fresh prepared mixture solution containing 400 mM EDC and 100 mM NHS for 30 min and then washed off. Then the Al NPA was covered with 50 μL CA199 antibody in PBS solution (1 mg/mL, pH=7.2) for 2 h and be washed thoroughly by PBS. After that, the antibody functionalized Al NPA was treated with 50 μL BSA solution (3 wt%) to block the excess active groups and nonspecific-binding site on the surface, and washed off. The Al NPA biosensor was dried with nitrogen flow and its reflectance was recorded as the reference. To detect CA199, the Al NPA biosensor was exposed to a 50 μL CA199 solution (100 ng/mL, pH 7.2) for 30 min, then washed cleanly and dried with nitrogen flow; the reflectance spectrum was recorded. To examine the anti-interference capability of the antibody functionalized Al NPA, we further exposed it into a mixture solution composed of CA199 (100 ng/mL) and alpha-fetoprotein (AFP, 100 ng/mL) and Cyt c (10 μM) for 30 min; after it was washed and dried, the reflectance spectrum was measured. All the spectral shift results were checked by comparing the reflectance spectra with the reference one. For concentration-dependent peak shift measurements, CA199 solutions with different concentrations of 20, 50, 100, 200, and 500 ng/mL were detected on different Al NPA substrates. At each concentration, three measurements were performed for the s.d. calculation.

3. Results

3.1. Al NPA fabrication

The Al NPA was prepared through a two-step procedure consisting of denting and then EC etching (Fig. 1A). Briefly, a polished Al sheet was dented using a Si mold with a square arranged array of nanopillars, and then was electrochemically anodized with stable high voltage to obtain ordered anodic alumina channels. The Al NPA substrate was obtained after the anodization layer was etched away. This method is simple and cost-effective, and has been widely used for Al nanostructures fabrication (Leung et al., 2012; Li et al., 2014; Lin et al., 2013a, 2013b; Norek et al., 2014). Fig. 1B is a side-view SEM image of the Al NPA which shows its morphology and structure. After anodizing and etching, the indentations were enlarged, and sharp pyramids formed at the juncture of each four adjacent indentations. The vertical height of the nanopyramid above the bottom of the indentation is 1.4 μm; the side length of the nanopyramid top is 100 nm. Fig. 1C is a top-view SEM image of Al NPA, showing that the nanopyramids are square arranged, with a lattice of 1.2 μm.

3.2. Tunable UV–vis-NIR wavelength plasmon resonances of the Al NPA

To understand the optical feature of the Al NPA, we measured its reflectance spectrum in air with incident angle ranging from 6° to 68° at a step of 1°. The reflectance spectra were recorded according to the measurement geometry illustrated as the inset in Fig. 2D. As it is showed in Fig. 2A, there are series of peaks distributing across the UV–vis-NIR region. The reflectance in UV and visible regions were much lower than that in NIR region. To see clearly the peaks locating at the UV to red wave regions, we divided the angle-resolved spectra into two wavelength intervals, which respectively were 200–500 nm and 500–900 nm. In Fig. 2B, we found UV-blue plasmon bands mainly existed at two angle intervals (between 8–46° and 65–68°), while visible and NIR plasmons could be found at all measuring angle (Fig. 2A and C). It has been known that the plasmons in Al nanostructures can be readily tuned into the UV plasmons compared with other metal (i.e. Au and Ag) nanostructures. To the best of our knowledge, this

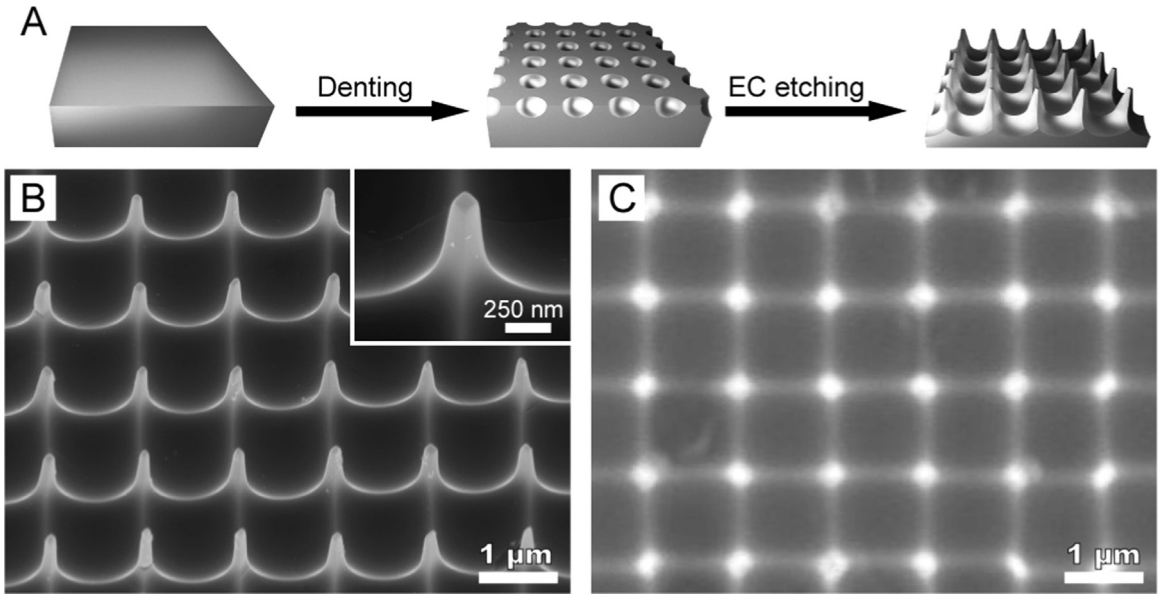

Fig. 1. Al NPAs. (A) Schematically illustrating the two-step fabrication procedure of aluminum NPA by imprinting and then EC etching. Scanning electron microscope (SEM) image showing (B) the side view and (C) the top view of the aluminum NPA. The inset in (B) is a magnification image of a typical NPA.

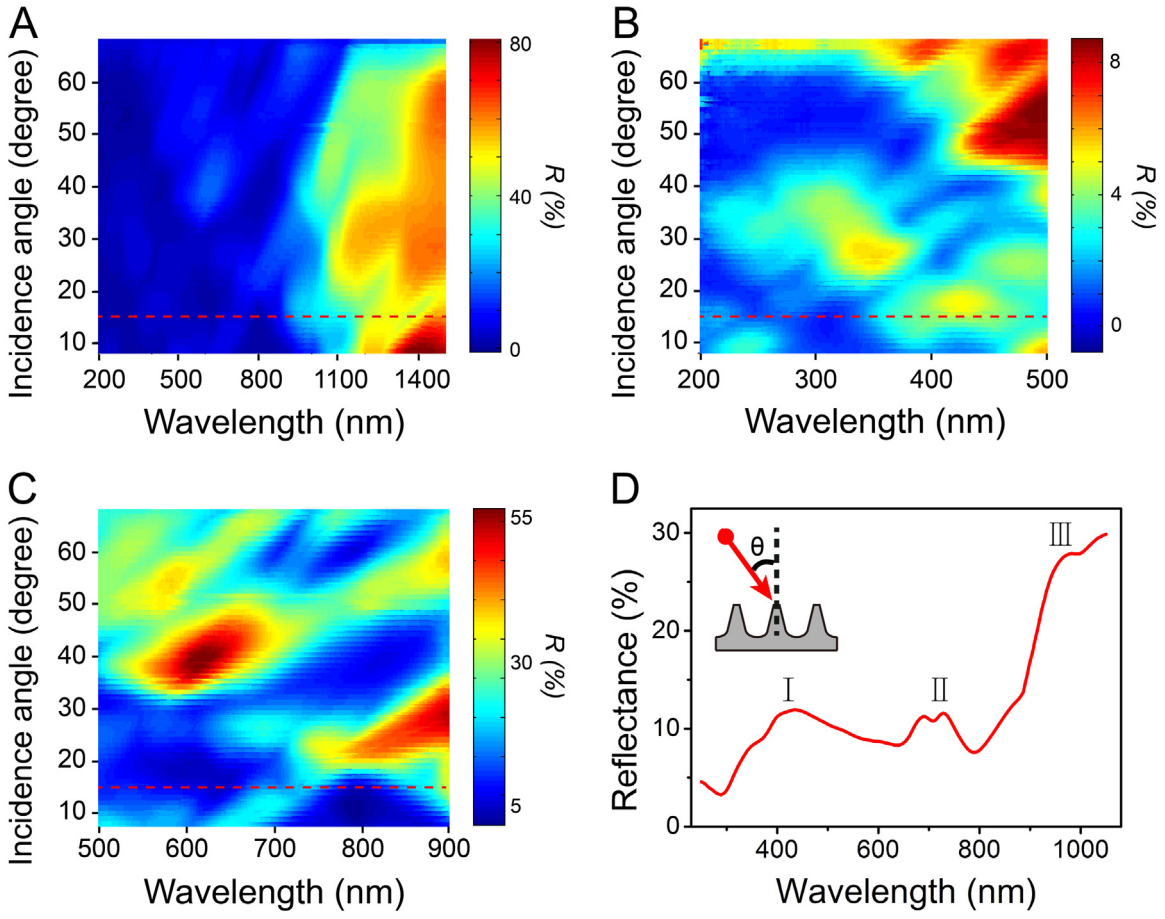

Fig. 2. Angle-resolved reflectance spectra of the Al NPA measured in air. (A) UV–vis-IR reflectance spectra for the incidence angle varied from 8° to 68° at a step of 1°. For clearly identification of the spectra in UV–vis region, the reflectance spectra are then divided into two wavelength intervals (B) from 200 to 500 nm, and (C) from 500 to 900 nm. The red dash line in (A), (B), and (C) denotes the angle of 15° for RI sensing. (D) Reflectance spectrum of the Al NPA at 15° incidence angle. The inset in (D) shows the reflectance measurement geometry.

is the first time that plasmons distributed across the whole UV–vis-IR wave band exhibited on one substrate were observed (Fig. S1), and can been effectively tuned by changing the incident angle. Fig. 2D showed the representative reflectance spectrum at a 15°-measuring angle, there are three peak groups simultaneously distributed at blue (groupI, λ=360–435 nm), red (group II, λ=670–850 nm), and infrared (group III, λ=950–1000 nm) wave regions, respectively.

3.3. RI sensing using Al NPA

To demonstrate the RI sensing properties of different peaks on its reflectance spectrum, we exposed the Al NPA into glycerine (GI)-water solution with different mixture ratio. As shown in Fig. 3, curve a) is the reflectance spectrum measured in air with a RI of 1.000, and curves b–f) are the reflectance spectra measured in GI–water mixtures with different mixture ratio and RI; the dip around 1420 nm is the absorption band of water. There are four dips and five peaks located on the spectra (D1, P1, D2, and P2 in group I; P3, D3, P4, and D4 in group II; and P5 in group III), as they are denoted on the magnified spectra of Al NPA in solutions (Fig. 3 B–C). These peaks and dips are all regularly redshifted as RIs in the surrounding medium are changed from 1.000 to 1.447, suggesting that the Al NPA substrate could be developed to be a RI sensor.

In order to calculate the RI sensitivities of the peaks and dips, we presented the normalized reflectance spectra of the Al NPA in the corresponding wave range with the increase in the RI of the surrounding environment. P2, P3, and D4 are taken as the representatives (Fig. 4 A–C). The spectral peak shifts of the biosensor against the RI are showed in Fig. 4D. In our case, the linear-fit RI sensitivities are 387 nm/RIU, 677 nm/RIU, and 819 nm/RIU for P2, P3, and D4, respectively. The RI sensitivity at D4 is even comparable with those of the typical noble metal plasmonic nanostructures (Chen et al., 2008; Nehl et al., 2006; Verellen et al., 2011; Wang et al., 2006), which, to our knowledge, may be the highest RI sensitivity of aluminum LSPRs demonstrated so far (Barrios et al., 2014; Canalejas-Tejero et al., 2014; Norek et al., 2014; Skinner et al., 2008). The high RI sensitivity of LSPR sensor is of importance to rapid detection of trace bio-analytes, enabling label-free and direct detection, which is inherently more time-saving and economic than sandwich-assays because it requires only single recognition element and provides direct detection without extensive protocols.

3.4. Al NPA for rapid bio-detection

To demonstrate the application of Al NPAs as refractometric biosensors, bio-functionalized Al NPAs were employed to detect Cyt c and CA 199 through nonspecific and specific interactions, respectively. Cyt c are critical proteins located in the mitochondrial intermembrane/intercristae spaces, where it functions as both an electron shuttle in the respiratory chain and inducement leading to apoptotic cell dismantling (Garrido et al., 2006). The detection of Cyt c has been extensively studied as a model system for biosensors (Song et al., 2004). For Cyt c detection, an UV-cleaned Al NPA was first PAA functionalized to generate pendent –COOH

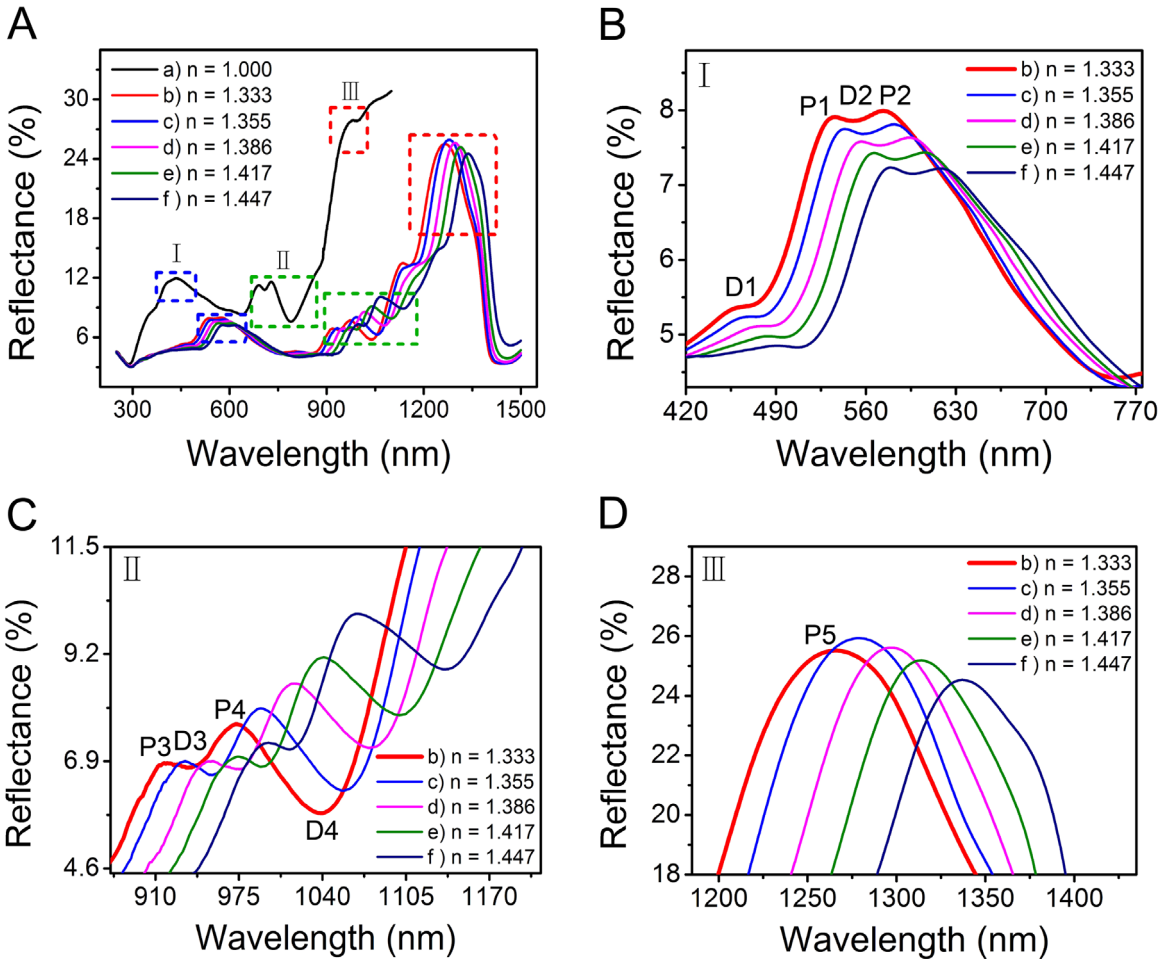

Fig. 3. Reflectance spectra of the Al NPA when it was exposed to (a) air and b–f) Gl–water mixtures with different mixture ratio. There are three peak groups (I, II, and III) distributed at UV, visible, and IR light region, respectively. The rectangles show the different plasmon resonance peaks red-shifted with the increase in the RI of the surrounding environment. (B–C) Reflectance spectra of the Al NPA immersed in GI–water solutions at peak group I, II, and III, as they are denoted by rectangles in (A).

groups through a self-assemble strategy. We monitored PAA modification of the NPA by checking its reflectance spectra every 5 min when it was immersed in Cyt c solution (10 mM, pH 7.2), and found that the optimized immersion time was 30 min (Fig. S2). As was showed in Fig. 5A, the reflectance spectrum of the newly PAA-modified NPA (black curve) was recorded as the reference, and Cyt c (10 μM and 35 μM as represents) adsorption led to different spectral redshfits of the peak D4. After each measurement, the PAA-modified NPA could be regenerated by washing it with an acidic PBS (pH 2.0) flow for 30 seconds. Fig. 5B shows the variation of the spectral position of the peak against Cyt c concentration. The red shift of the peak ranges from 0.4 to 7.2 nm as Cyt c concentration is increased from 0.5 to 35 μM. The LOD is determined to be 0.8 μM (S/N=3). It is worth mentioning that the concentration of Cyt c in aqueous solution also can be detected by measuring its optical absorbance at 550 nm on a spectrometer. Compared with the method based on optical absorbance, the proposed transduction is real-time and less-sample-consumption (~20 μL). Furthermore, if immunoassay system is employed to the system, we could achieve biosensing with high selectivity.

CA199 was chosen to demonstrate that the Al NPA substrate is also applicable for specific bio-sensing which involves more complex interactions. CA199 is a biomarker specific to cancer exists in the digest system (Zhou et al., 2012), such as pancreatic cancer, colorectal cancer, and gastric cancer. The concentration of CA199 in serum is normally bellow 35 ng/mL, but increases remarkably during the diseases state. To detect CA199, the Al NPA was previously functionalized with CA199 antibody (Fig. S3). Fig. 5C show the reflectance spectra when the Al NPA biosensor was incubated in PBS solution, 3.0 wt% BSA solution, 200 ng/mL CA199 solution, and a mixture solution containing CA199 (200 ng/mL), Cyt c (10 μM), and alpha-fetoprotein (200 ng/mL), respectively. The extracted peak positions were plotted in Fig. S4. BSA is a commonly blocking agent (Wang et al., 2013) used for biosensing. The reflectance spectrum of the Al NPA showed no observable redshift after it was incubated in BSA solution for 30 min, indicating an excellent anti-interference capability of our Al NPA biosensor (Dai et al., 2006). The spectrum was redshifted 3.2 nm after it was exposed to CA199 solution, and no further shift was observed when the Al NPA biosensor was immersed in the mixture solution. This demonstrates that, on one hand, the immuno-binding between CA199 antigen and antibody has been saturated in 30 min, on the other one hand, the electronic absorption of conventional biomolecules and cross-talk caused from other cancer biomarker are both avoided; the Al NPA biosensor showed excellent selectivity. Fig. 5D plots the concentration-dependent peak shift for the CA199 detection, the peak red shifted from 0.95 to 4.8 nm with the concentration of the CA199 increased from 20 to 400 ng/mL, with the limit of detection (LOD) estimated to be 29 ng/mL. The obtained LOD is below the critical concentration (~35 ng/mL) in normal plasma suggested by Sun Yat-sen University Cancer Center. These results suggest that the Al NPA offers a state-of-art system for label-free and one-step rapid biodetection.

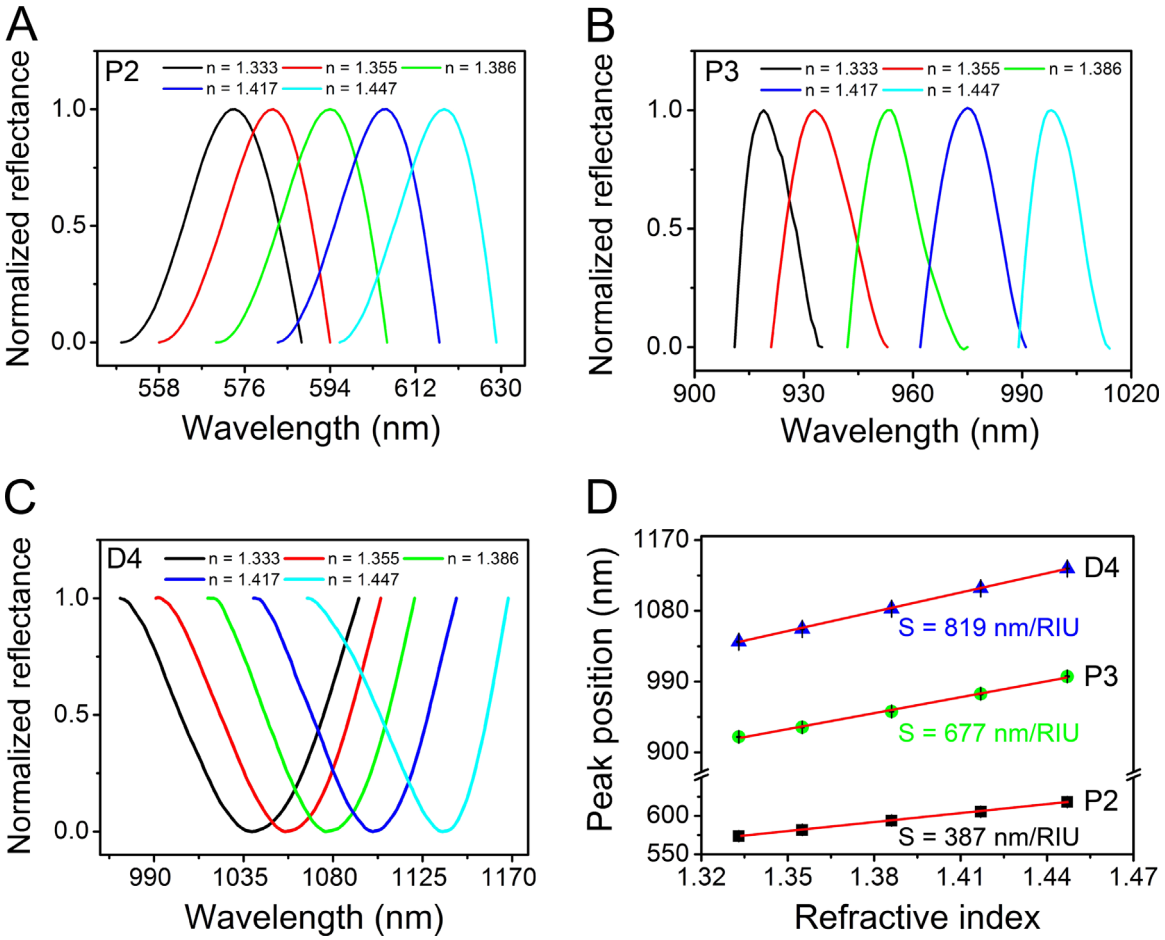

Fig. 4. RI sensing using different peaks and dips on the reflectance spectrum of the Al NPA substrate. (A–C) RI-resolved normalized reflectance spectra of the Al NPA at P2, P3, and D4. (D) Relationship between the positions of the P2, P3, and D4 and the RIs. The red lines are linear fits. The error bars are two small to been seen. (For interpretation of the references to color in this figure legend, the reader is referred to the web version of this article.)

4. Discussion

We fabricated a Quasi-3-demonsional Al NPA structure through a two-step procedure consisting of denting and then EC etching. This method is simple and cost-effective. The Al NPA was demonstrated to be has series of peaks/dips distributing across the UV–vis-NIR region, and both the number of these peaks/dips and their locations was varied as the measuring angle changed. It worth mentioning that, due to the very low reflectance in UV to visible regions, the NPA could be further developed for photovoltaic applications.

We measured the RI sensitivities of all peaks and dips at a measuring angle of 15°, and found that, as the plasmon resonance position located at longer wavelength, the corresponding peak/dip shows higher RI sensitivity (Fig. 6). Note that, the left shoulders of P5 in solutions overlapped with the absorption band of the GI–water mixture, which makes the RI sensitivity unreliable at this wavelength. The sensitivity of D4 is even comparable with those of the typical noble metal plasmonic nanostructures[36-39], which, to our knowledge, may be the highest RI sensitivity of aluminum LSPRs demonstrated so far. Such a high sensitivity initiates label-free and one-step detection of trace cancer biomarkers in corresponding to that in normal human serum.

In our case, all measurements were performed in air after the surface of the Al NPA biosensor was washed thoroughly and dried with nitrogen flow, which are more accurate and sensitive (Li et al., 2015). While we should note that, measurement of Al NPA could be in solution and also has many applications, such as detection of analytes and real-time monitoring of molecular binding. Moreover, Al NPA offers several other advantages for biosensing. (1) The Al NPA is very stable, due to the presence of a thin oxide layer (Langhammer et al., 2008), which is about 2.5 nm according to the angle-resolved X-ray photoelectron spectroscopy analysis (Fig. S5A). We put the Al NPA in air for 3 weeks, and treated its surface repeatedly with O_2 plasma and UV ray at intervals, and found the reflectance spectra were almost the same with the initial one (Fig. S5B), suggesting that the Al NPA is well protected by the oxide layer on its surface (Knight et al., 2014; Norek et al., 2014). (2) The LSPR features of the NPA employed for biosensing therefore would not be influenced by slight changes or damages in the top of the nanopyramid, which are most likely bumped in the measurement operation; The finite difference time domain simulation at 15°-incidences angle showed that, the electric intensity of the NPA was mainly distributed at the side edges of the nanopyramid and the bottom of the indentations, while there was little at the corners of the top (Fig. S6). (3) Al NPA enables high throughput sensing. We checked the reflectance spectra at 6 locations on the Al NPA surface with an area of 7×6 mm^2, and found that the positions of the peaks were almost the same (Fig. S7). Both the spectral results and the SEM images show that Al NPA has a large-area and uniform nanostructure, which will be beneficial for high throughput screening on single Al NPA substrate.

5. Conclusions

We have demonstrated a uniform quasi-3-dimensional Al nanopyramid array (NPA) structure with tunable UV–vis-NIR plasmon

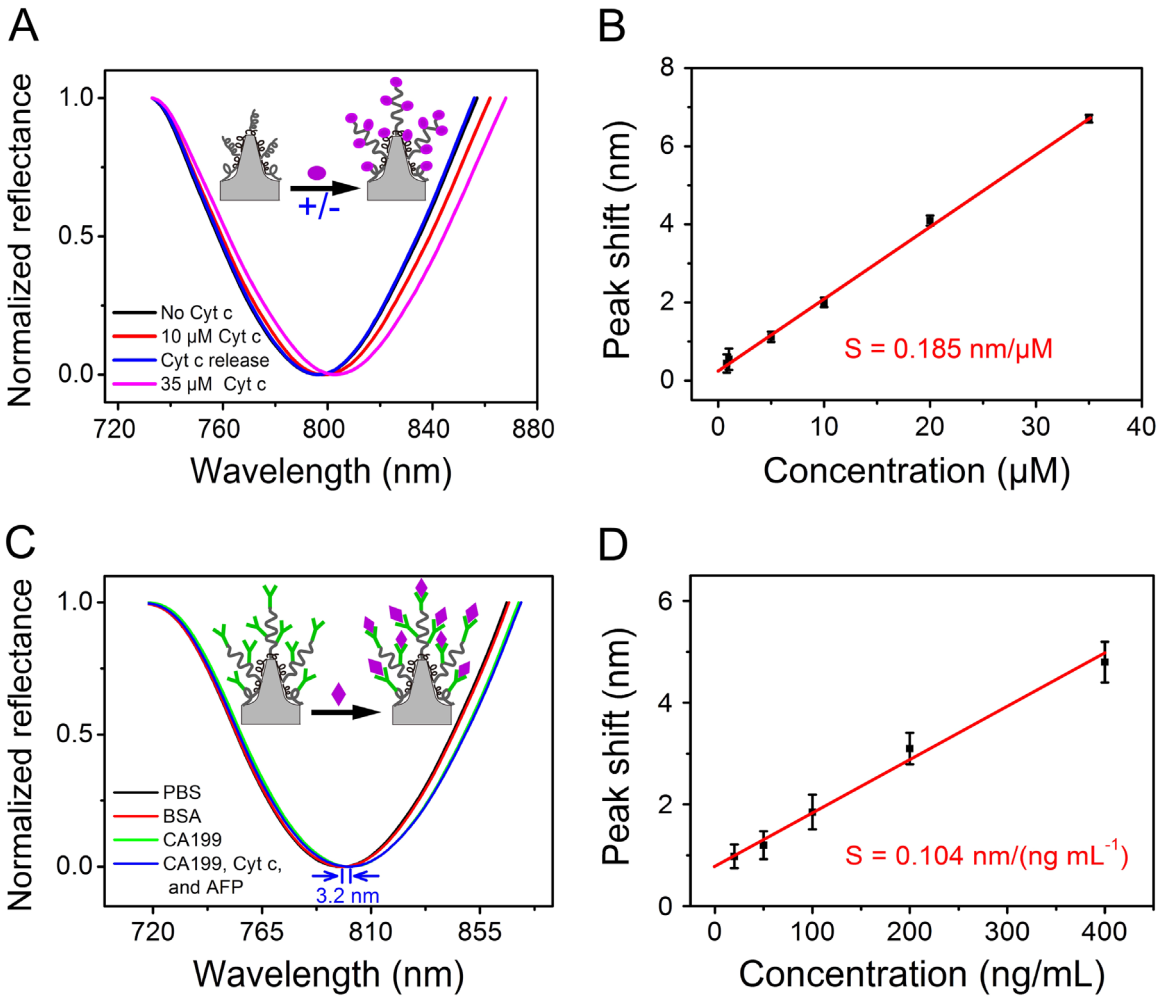

Fig. 5. Label-free and one-step detection of Cyt c and CA199. (A) Representative reflectance spectra for detecting Cyt c on the PAA-modified Al nanopyramid by non-specific interaction; the array surface was regenerated in PBS (pH 2.0) after the adsorption at each concentration. The spectrum (black) recorded without Cyt c treatment and that (blue) acquired after the regeneration from the adsorption at 35 μM are provided for references. (B) Relationship between the dip shift and Cyt c concentration. The inset in (A) illustrates the Cyt c detection through electrostatic interaction using PAA modified NPA. (C) Representative reflectance spectra for detecting CA199 on the anti-CA199 modified Al nanopyramid by specific interaction; the antibody-functionalized Al NPA was incubated in PBS (pH 7.2), BSA (3.0 wt%) solution, CA199 (200 ng/mL) solution, and a mixture solution containing CA199 (200 ng/mL), Cyt c (10 μM), and AFP (200 ng/mL). (D) Relationship between the dip shift and the CA199 concentration. The inset in (C) illustrates the direct detection of CA199 via immunobinding on antibody functionalized Al NPAs.

resonance for biosensing. By changing the reflection measuring angle, we easily obtain LSPR peaks simultaneously exhibited on the reflectance spectrum from UV–vis to infrared wave region. The Al NPA holds high RI sensitivity which is even comparable with that of noble metal, and can be used as a biosensor for detecting cytochrome c (Cyt c) and carbohydrate antigen 199 (CA199), with limits of detection determined to be 800 nM and 29 ng/mL, respectively. To the best of our knowledge, this is the first time that, on one hand, metal nanostructure with plasmon bands simultaneously distributed across the UV–vis-NIR region has been found; on the other hand, Al plasmonic substrate was succeeded in rapid, direct detection of cancer biomarker when its surface was well functionalized. Our proposed work therefore initiates the low-cost, high-performance biosensing using aluminum materials, which would find wide applications in rapid diagnosis and mobile-healthcare on microfluidic chips.

Author contributions

J.H.Z. and W.B.L. designed research; W.B.L., Y.C.Q., L.Z. and L.L.J. performed research; Z.K.Z. and H.J.C. performed FDTD simulations; J.H.Z., and W.B.L. performed data analyses; J.H.Z., W.B.L., H.J.C. and Z.K.Z. wrote the manuscript. All authors read and commented on the manuscript.

Acknowledgments

This work was supported in part by the National Natural Science Foundation of China (21405183), the project for Science & Technology New Star of Zhujiang in Guangzhou City (2013J2200048) and the project supported by the Guangzhou Science and Technology and Information Bureau (2014J4100108). The work was also supported in part by the Australia-China Joint Institute for Health Technology and Innovation (startup funding, 2015).

Appendix A. Supplementary material

Supplementary data associated with this article can be found in the online version at http://dx.doi.org/10.1016/j.bios.2015.12.038.

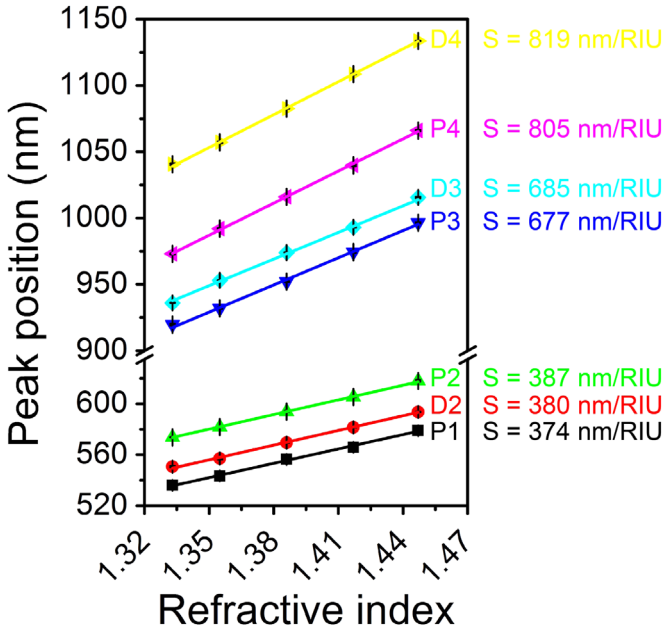

Fig. 6. RI-resolved positions of the peaks and dips at a measuring angle of 15°. The lines are linear fits. Some Error bars are too small to be seen.

References

Ament, I., Prasad, J., Henkel, A., Schmachtel, S., Sönnichsen, C., 2012. Nano Lett. 12, 1092–1095.
Atwater, H.A., Polman, A., 2010. Nat. Mater. 9, 205–213.
Barrios, C.A., Canalejas-Tejero, V., Herranz, S., Moreno-Bondi, M.C., Avella-Oliver, M., Puchades, R., Maquieira, A., 2014. Plasmonics 9, 645–649.
Bisio, F., Proietti Zaccaria, R., Moroni, R., Maidecchi, G., Alabastri, A., Gonella, G., Giglia, A., Andolfi, L., Nannarone, S., Mattera, L., Canepa, M., 2014. ACS Nano 8, 9239–9247.
Canalejas-Tejero, V., Herranz, S., Bellingham, A., Moreno-Bondi, M.C., Barrios, C.A., 2014. ACS Appl. Mater. Inter. 6, 1005–1010.
Chan, G.H., Zhao, J., Schatz, G.C., Duyne, R.P.V., 2008. J. Phys. Chem. C 112, 13958–13963.
Chen, H., Kou, X., Yang, Z., Ni, W., Wang, J., 2008. Langmuir 24, 5233–5237.
Chowdhury, M.H., Ray, K., Gray, S.K., Pond, J., Lakowicz, J.R., 2009. Anal. Chem. 81, 1397–1403.
Clausen, J.S., Højlund-Nielsen, E., Christiansen, A.B., Yazdi, S., Grajower, M., Taha, H., Levy, U., Kristensen, A., Mortensen, N.A., 2014. Nano Lett. 14, 4499–4504.
Dai, J., Baker, G.L., Bruening, M.L., 2006. Anal. Chem. 78, 135–140.
Free, C., Phillips, G., Watson, L., Galli, L., Felix, L., Edwards, P., Patel, V., Haines, A., 2013. Plos Med. 10, e1001363.
Garrido, C., Galluzzi, L., Brunet, M., Puig, P.E., Didelot, C., Kroemer, G., 2006. Cell. Death Differ. 13, 1423–1433.
Gordon, R., Sinton, D., Kavanagh, K.L., Brolo, A.G., 2008. Accounts Chem. Res. 41, 1049–1057.
Guo, L., Kim, D., 2011. Chem. Commun. 47, 7125.
Knight, M.W., King, N.S., Liu, L., Everitt, H.O., Nordlander, P., Halas, N.J., 2014. ACS Nano 8, 834–840.
Langhammer, C., Schwind, M., Kasemo, B., Zorić, I., 2008. Nano Lett. 8 1461-11471.
Leung, S., Yu, M., Lin, Q., Kwon, K., Ching, K., Gu, L., Yu, K., Fan, Z., 2012. Nano Lett. 12, 3682–3689.
Li, J., Qiu, Y., Wei, Z., Lin, Q., Zhang, Q., Yan, K., Chen, H., Xiao, S., Fan, Z., Yang, S., 2014. Energy Environ. Sci. 7, 3651–3658.
Li, W., Jiang, X., Xue, J., Zhou, Z., Zhou, J., 2015. Biosen. Bioelectron. 68, 468–474.
Liao, P.F., Stern, M.B., 1982. Opt. Lett. 7, 483–485.
Lin, Q., Hua, B., Leung, S., Duan, X., Fan, Z., 2013. ACS Nano 7, 2725–2732.
Lin, Q., Leung, S.F., Tsui, K.H., Hua, B., Fan, Z., 2013. Nanoscale Res. Lett. 8, 268.
Lohse, S.E., Burrows, N.D., Scarabelli, L., Liz-Marzán, L.M., Murphy, C.J., 2014. Chem. Mater. 26, 34–43.
Naik, G.V., Shalaev, V.M., Boltasseva, A., 2013. Adv. Mater. 25, 3264–3294.
Nehl, C.L., Liao, H., Hafner, J.H., 2006. Nano Lett. 6, 683–688.
Norek, M., Włodarski, M., Matysik, P., 2014. Curr. Appl. Phys. 14, 1514–1520.
O Brien, M.N., Jones, M.R., Brown, K.A., Mirkin, C.A., 2014. J. Am. Chem. Soc. 136, 7603–7606.
Olson, J., Manjavacas, A., Liu, L., Chang, W., Foerster, B., King, N.S., Knight, M.W., Nordlander, P., Halas, N.J., Link, S., 2014. P. Natl. Acad. Sci. USA 111, 14348–14353.
Ray, K., Chowdhury, M.H., Lakowicz, J.R., 2007. Anal. Chem. 79, 6480–6487.
Sannomiya, T., Vörös, J., 2011. Trends Biotechnol. 29, 343–351.
Schade, M., Fuhrmann, B., Bohley, C., Schlenker, S., Sardana, N., Schilling, J., Leipner, H.S., 2014. J. Appl. Phys. 115, 84309.
Schuller, J.A., Barnard, E.S., Cai, W., Jun, Y.C., White, J.S., Brongersma, M.L., 2010. Nat. Mater. 9, 193–204.
Skinner, J.L., Hunter, L.L., Talin, A.A., Provine, J., Horsley, D.A., 2008. IEEE T. Nanotechnol. 7, 527–531.
Song, J.M., Kasili, P.M., Griffin, G.D., Vo-Dinh, T., 2004. Anal. Chem. 76, 2591–2594.
Stewart, M.E., Mack, N.H., Malyarchuk, V., Soares, J.A., Lee, T.W., Gray, S.K., Nuzzo, R. G., Rogers, J.A., 2006. Proc. Natl. Acad. Sci. USA 103, 17143–17148.
Tan, S.J., Zhang, L., Zhu, D., Goh, X.M., Wang, Y.M., Kumar, K., Qiu, C., Yang, J.K.W., 2014. Nano Lett. 14, 4023–4029.
Verellen, N., Van Dorpe, P., Huang, C., Lodewijks, K., Vandenbosch, G.A.E., Lagae, L., Moshchalkov, V.V., 2011. Nano Lett. 11, 391–397.
Wang, C., Zhang, Q., Song, Y., Chou, S.Y., 2014. ACS Nano 8, 2618–2624.
Wang, G., Qing, Y., Shan, J., Jin, F., Yuan, R., Wang, D., 2013. Microchim. Acta 180, 651–657.
Wang, H., Brandl, D.W., Le, F., Nordlander, P., Halas, N.J., 2006. Nano Lett. 6, 827–832.
Yokogawa, S., Burgos, S.P., Atwater, H.A., 2012. Nano Lett. 12, 4349–4354.
Zhang, X., Zhao, J., Whitney, A.V., Elam, J.W., Van Duyne, R.P., 2006. J. Am. Chem. Soc. 128, 10304–10309.
Zheng, B.Y., Wang, Y., Nordlander, P., Halas, N.J., 2014. Adv. Mater. 26, 6318–6323.
Zhou, G., Niu, L., Chiu, D., He, L., Xu, K., 2012. Biotechnol. Lett. 34, 1235–1241.